PHYSICAL REVIEW B **91**, 235137 (2015)

# Optical dielectric function of silver

Honghua U. Yang,[1] Jeffrey D'Archangel,[2] Michael L. Sundheimer,[3] Eric Tucker,[4]
Glenn D. Boreman,[4] and Markus B. Raschke[1,*]

[1]*Department of Physics, Department of Chemistry, and JILA, University of Colorado, Boulder, Colorado 80309, USA*
[2]*CREOL, College of Optics & Photonics, University of Central Florida, 4304 Scorpius Street, Orlando, Florida 32816, USA*
[3]*Department of Physics, Universidade Federal Rural de Pernambuco, Recife, Brazil*
[4]*Department of Physics and Optical Science, University of North Carolina, Charlotte, North Carolina 28223, USA*

(Received 14 January 2015; revised manuscript received 31 March 2015; published 22 June 2015)

The dielectric function of silver is a fundamental quantity related to its electronic structure and describes its optical properties. However, results published over the past six decades are in part inconsistent and exhibit significant discrepancies. The measurement is experimentally challenging with the values of dielectric function spanning over five orders of magnitude from the mid-infrared to the visible/ultraviolet spectral range. Using broadband spectroscopic ellipsometry, we determine the complex-valued dielectric function of evaporated and template stripped polycrystalline silver films from 0.05 eV ($\lambda = 25\ \mu$m) to 4.14 eV ($\lambda = 300$ nm) with a statistical uncertainty of less than 1%. From Drude analysis of the 0.1–3 eV range, values of the plasma frequency $\hbar\omega_p = 8.9 \pm 0.2$ eV, dielectric function at infinite frequency $\epsilon_\infty = 5 \pm 2$, and relaxation time $\tau = 1/\Gamma = 17 \pm 3$ fs are obtained, with the absolute uncertainties estimated from systematic errors and experimental repeatability. Further analysis based on the extended Drude model reveals an increase in $\tau$ with decreasing frequency in agreement with Fermi liquid theory, and extrapolates to $\tau \simeq 22$ fs for zero frequency. A deviation from simple Fermi liquid behavior is suggested at energies below 0.1 eV ($\lambda = 12\ \mu$m) with the onset of a further increase in $\tau$ connecting to the DC value from transport measurements of $\sim 40$ fs. The results are consistent with a wide range of optical and plasmonic experiments throughout the infrared and visible/ultraviolet spectral range. However, due to the polycrystalline nature of our sample, the values measured are not likely reaching the intrinsic limit of silver. The influence of grain boundaries, defect scattering, and surface oxidation is discussed. The results are compared with our previous measurements of the dielectric function of gold [Olmon *et al.*, Phys. Rev. B **86**, 235147 (2012)].

DOI: 10.1103/PhysRevB.91.235137 PACS number(s): 78.20.Ci, 78.30.Er

## I. INTRODUCTION

Knowledge of the frequency-dependent dielectric function gives insight into the underlying elementary excitations of materials, such as lattice vibrations, free carrier absorption, superconducting gaps, plasmon resonances, chemical bonding, excitons, or interband absorption [1–3]. The dielectric function also directly relates to many optical properties, in particular transmission, reflection, and dispersion at the most fundamental level. The dielectric function of silver together with that of other noble metals has played an important historical role in the understanding of the electronic structure of metals [4–8]. This role continues for understanding the ultrafast electron dynamics of metals [9–15]. Silver in particular assume a special status due to its high optical conductivity and wide range of applications from mirrors to plasmonics and optical metamaterials.

However, similarly to the case of gold [16], large variations exist among historical measurements of the dielectric function of silver, especially for the imaginary part near the interband transition in the visible/ultraviolet (visible/UV) region [17]. Most of these measurements only cover a narrow energy range, making a direct comparison between the different experiments difficult. In addition, discrepancies between theoretical and experimental values of different optical and plasmonic properties of silver have raised concerns over the accuracy of some of the most widely used measurements of the dielectric function of silver [18–27]. Accurate values for the dielectric function of silver are needed in the visible and infrared (IR) spectral ranges, because many important parameters, such as surface plasmon propagation length, plasmon lifetime, nonradiative loss, and even the Casimir force, are sensitively linked to small variations of the dielectric function [16].

In this work, we provide a comprehensive measurement of the optical dielectric function $\epsilon(\omega)$ of evaporated and template-stripped polycrystalline silver using spectroscopic ellipsometry, covering a broad spectral range throughout the mid-IR to visible/UV of two orders of magnitude, from 0.05 eV to 4.14 eV (25 $\mu$m to 300 nm). We analyze the free electron behavior below the interband transition using the Drude model with plasma frequency $\omega_p$, dielectric function at infinite frequency $\epsilon_\infty$, and relaxation time $\tau = 1/\Gamma$. While there is a good agreement of $\omega_p$ and $\epsilon_\infty$ with many past measurements, our value of $\tau = 17 \pm 3$ fs is significantly shorter than the commonly used literature value from Johnson and Christy of $31 \pm 12$ fs [28] and the value derived from DC conductivity of ~40 fs [29,30], yet consistent with most optical and plasmonic experiments, such as typical surface plasmon propagation length and particle plasmon resonance lifetimes [21,23,25,31,32]. The difference in $\tau$ between the DC and the optical frequency measurements is due to the frequency dependence of the scattering rate $1/\tau(\omega)$ [33,34]. An analysis with the extended Drude model extracts this frequency dependence, which is found to be consistent with Fermi liquid theory beyond 0.1 eV [33,35,36]. However, at energies below 0.1 eV $\tau(\omega)$ rises more rapidly than suggested by the Fermi liquid theory possibly connecting to the Drude DC value of

*markus.raschke@colorado.edu

 

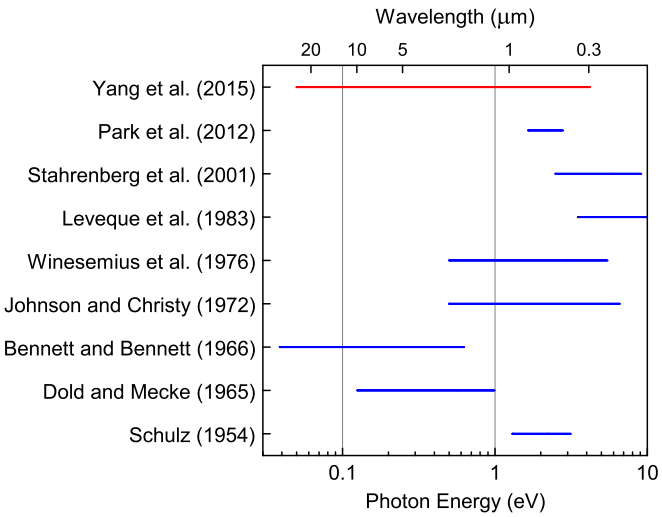


FIG. 1. (Color online) Six decades of dielectric function measurements of Ag covering different spectral regions, with in part inconsistent results mostly notably in the visible/UV spectral range. Our measurement broadly covering the mid-IR to visible/UV range is shown in red.

40 fs. We discuss effects of impurity and grain boundary scattering, and note that even for samples prepared under nominally identical conditions, sample-to-sample variations can be as large as 30% for the imaginary part $\epsilon_2$ near the interband transition. Due to impurity and surface defect scatterings in our samples, the Drude relaxation time of $\tau = 17 \pm 3$ fs may not represent the intrinsic limit of silver. Single crystal samples with low defect and impurity levels may be needed for further studies [26,37].

### A. Past measurements of dielectric function

Many previous experiments have measured the dielectric function of silver, based on different methods, and with partially inconsistent values. Figure 1 shows selected examples of studies representative of the different experimental methods and measurement ranges, with the spectral range and the year of publication. For comparison, our measurements range are shown in red.

Various measurement techniques and deposition methods have been employed in previous measurements [17,38–40]. Drude's polarimetric methods were used in early studies of evaporated metallic thin films. For example, reflectance measurements with different polarizations were carried out by Dold and Mecke on evaporated silver on polished glass to determine $n$ and $k$ in the range of 0.13–1 eV [41]. The same measurement method was applied to polycrystalline silver by Winsemius *et al.* in vacuum covering 0.5–5.4 eV [42]. An interferometric method was developed by Schulz to determine the absorption coefficient $k$ from the phase change of reflection at normal incidence from 1.3 to 3.1 eV [43,44]. More specifically, Ag-$x$-Ag multilayers were used in his experiment with $x$ being mica or other dielectric material. In a separate study Schulz calculated index of refraction $n$ from measured reflectivities at an incidence angle of 45° with a predetermined absorption coefficient $k$ from the above multilayer measurement [45]. The most common method to obtain the dielectric function is to apply Kramers-Kronig analysis on reflectance or transmission spectra of silver films. Hagemann *et al.* performed transmission measurements on evaporated silver thin films on collodion substrates in the range of 13–150 eV [46]. The resulting spectrum was complemented with other data in the literature to yield a broad spectral range for proper Kramers-Kronig analysis. Similar measurements of silver films were carried out by Leveque *et al.* in vacuum after sample evaporation in the same chamber without exposing to air [47]. The reflectance spectrum from 3.5 to 30 eV was again extended with other data from literature for a Kramers-Kronig analysis. Similarly, Quinten developed a method for determining the dielectric function of metallic clusters from Kramers-Kronig analysis of optical extinction spectra [18]. Combined reflectance and transmittance measurements of semitransparent thin films prepared by evaporation on fused quartz were done by Johnson and Christy in the range of 0.5–6.5 eV [28]. In their work, contour plots of the reflectance and transmittance were used to determine the complex index of refraction $\tilde{n}(\omega) = n(\omega) + ik(\omega)$. In the visible spectral range from 1.38 to 2.76 eV, angle-dependent surface plasmon-polariton resonance on a silver-covered silica grating were used by Nash and Sambles to calculate the dielectric function [19]. More recently, spectroscopic ellipsometry was used to obtain the dielectric function with improved acquisition speed and accuracy over a broad spectral range limited only by light sources and detectors [48]. Stahrenberg *et al.* prepared clean surfaces of single-crystal Ag *in situ* by ion sputtering and annealing [49]. Subsequent ellipsometry measurements were taken in the same ultrahigh vacuum environment in the spectral range of 2.5–9.0 eV using a synchrotron light source. Park *et al.* measured template stripped silver with reduced roughness by ellipsometry in the visible spectral range of 1.65–2.75 eV [31,37].

Large inconsistencies between the different measurements exist and were noted early, and suggested to be due to sample contamination [50,51], differences in surface morphologies [52,53], strain [47,54], and the different measurement techniques [16]. Some data even appear unphysical with noted anomalies such as a broad peak in the reflectance spectrum at 5 $\mu$m [41]. Here, the cause was attributed to erroneously low values measured for $k$ by Lynch and Hunter [17].

Only one previous measurement has yet addressed the low-energy range below 0.2 eV (>6 $\mu$m) [55]. In that study, reflectance at normal incidence was measured in the 3–30 $\mu$m wavelength range by Bennett and Bennett. The experimental reflectivity was compared to the calculated reflectivity from the Drude model with good agreement. However, since reflectivity itself is not sufficient to constrain the three parameters in the Drude model, a value of $\tau = 36$ fs based on DC conductivity was assumed for data modeling.

### B. Dielectric function and Drude model

The dielectric function of a medium, determined by its intrinsic electronic structure, is given by [2,3]

$$D_i(r,t) = \iint \epsilon_{ij}(r,r',t,t')E_j(r',t')dt'dr', \qquad (1)$$

where the components of displacement field $D_i$ and electric field $E_j$ and are related through the dielectric tensor $\epsilon_{ij}$. Within the local response approximation and in a homogeneous medium, Eq. (1) simplifies to

$$D_i(r,t) = \int \epsilon_{ij}(t-t')E_j(r,t')dt', \tag{2}$$

or in the frequency domain

$$D_i(r,\omega) = \epsilon_{ij}(\omega)E_j(r,\omega). \tag{3}$$

Silver, being a face-centered-cubic crystal lattice, is optically isotropic [56,57]. As a result, the dielectric function can be expressed by a scalar $\epsilon(\omega) = \epsilon_0\epsilon_r(\omega)$, where $\epsilon_0$ is the vacuum permittivity and $\epsilon_r(\omega)$ is the relative dielectric function. Thus $\epsilon_r(\omega)$ describes the full electromagnetic response of the medium in the absence of magnetic effects.

The relative dielectric function $\epsilon_r(\omega) = \epsilon_1(\omega) + i\epsilon_2(\omega)$ relates to the index of refraction through $\tilde{n}(\omega) = n(\omega) + ik(\omega) = \sqrt{\epsilon_r(\omega)}$. For a metal, the dielectric function also defines the frequency-dependent complex conductivity $\sigma(\omega) = \sigma_1(\omega) + i\sigma_2(\omega) = -i\epsilon_0\omega[\epsilon_r(\omega) - 1]$, where the real part $\sigma_1(\omega)$ describes the ohmic loss and the imaginary part $\sigma_2(\omega)$ defines the phase lag between the applied electric field and the electric current.

In the low-energy region, where electronic intraband transitions within the conduction band dominate, the dielectric function of a metal can be described to a good approximation as a gas of noninteracting electrons by the *Drude-Sommerfeld* free electron model (denoted as Drude model below). In the Drude model the equation of motion for the conduction electrons driven by a time-harmonic field is solved for $\epsilon_r(\omega)$ as a response function, with

$$\epsilon_r(\omega) = \epsilon_\infty - \frac{\omega_p^2}{\omega^2 + i\omega\Gamma}, \tag{4}$$

where the volume plasma frequency $\omega_p$ is related to the effective mass of the electron $m^*$ and the electron density $N$ through $\omega_p = (Ne^2/\epsilon_0 m^*)^{1/2}$. The relaxation rate $\Gamma$ describes the effective electron scattering rate, with a corresponding relaxation time $\tau = 1/\Gamma$. The parameter $\epsilon_\infty$ accounts for the net contribution from the positive ion cores. For the ideal free electron gas $\epsilon_\infty = 1$, and for typical metals $\epsilon_\infty = 1$–$10$ depending on the interband response [8,58]. The contribution to the dielectric function from the interband transition of $d$ band to $sp$ band can empirically be accounted for by functions of damped harmonic oscillators [33,59].

The dielectric function $\epsilon_r(\omega)$ in Eq. (4) can be decomposed into real $\epsilon_1$ and imaginary part $\epsilon_2$, with

$$\epsilon_1(\omega) = \epsilon_\infty - \frac{\omega_p^2}{\omega^2 + \Gamma^2} \approx \epsilon_\infty - \frac{\omega_p^2}{\omega^2}, \tag{5}$$

$$\epsilon_2(\omega) = \frac{\omega_p^2 \times \Gamma}{\omega(\omega^2 + \Gamma^2)} \approx \frac{\omega_p^2 \times \Gamma}{\omega^3}, \tag{6}$$

with the approximations valid for $\omega \gg \Gamma$. Equations (5) and (6) allow for the direct calculations of $\omega_p$, $\epsilon_\infty$, and $\Gamma$ from $\epsilon_1(\omega)$ and $\epsilon_2(\omega)$ for large frequencies, as shown below.

The Drude model provides an effective description of the free carrier response in metals, but it neglects band structure effects and also provides no physical insight into the underlying electron interactions [2,56]. Band structure effects need to be accounted for in calculation to reproduce the correct position of the plasmon resonance in silver [60]. Dynamic exitonic and quasiparticle effects are responsible for a correct renormalization factor in the energy loss function $\mathrm{Im}[1/\epsilon]$ [10,11,60]. The underlying electron interactions can be modeled with Fermi liquid theory, which mathematically transforms the strongly interacting electrons into free quasiparticles [61]. Quasiparticles are a simplified way to describe the collective motion of electrons due to many-body effects. The physics lies in the small probability to change the momentum distribution of quasiparticles near the Fermi surface due to Pauli blocking. As a result, the free quasiparticle picture can explain the macroscopic response of the interacting electron system with frequency-dependent renormalized effective electron mass $m^*$ and relaxation time $\tau$ [35,61]. In addition to these intrinsic effects, the Drude model has to be further modified by extrinsic effects such as surface, impurity, and grain boundary scattering.

Deviations from the Drude model have been noticed in recent experiments due to both intrinsic and extrinsic effects, including band structure, impurity, and surface effects [62–64]. In the study of DC conductivity of metals, intrinsic effects can be determined after consideration of extrinsic effects from systematic studies under controlled temperature and impurity levels [30,65,66]. In contrast, the determination of the spectroscopic behavior of the dielectric function at optical frequencies is more involved. However, with an accurate measurement of the dielectric function of the most commonly used form of the metal over a broad spectral range, we can quantitatively compare the experimental dielectric function with different models and literature, thus posing constraints on intrinsic and extrinsic effects.

## II. EXPERIMENT

Template stripped (TS) silver films deposited on Si substrates were chosen for spectroscopic ellipsometry measurement over the range of 0.05–4.14 eV. The experimental procedure is generally similar to our previous measurements on gold [16]. The deposition of the metal on a flat substrate (template) leads to a smooth and more homogeneous metal surface at the metal-substrate interface compared to the vacuum side of the film. The metal film can then be stripped off the substrate to reveal the desired surface. For template stripping we use a silicon wafer with a native oxide layer ($Si/SiO_2$) (University Wafer) as substrate, ultrasonically cleaned in isopropyl alcohol and dried with nitrogen. Silver pellets of 99.99% pure element (Kurt J. Lesker) are evaporated in a cryopumped evaporator (E360A, Edwards) from a molybdenum boat at a pressure of $<10^{-6}$ mbar. A silver film of thickness 150 nm (optically opaque and thick enough to resemble the bulk properties of silver through most of the spectral region studied) is deposited at a rate of 0.1–0.2 nm/s. The substrate is not heated during evaporation. In order to transfer and expose the desired metal surface after evaporation, the sample is glued with the vacuum silver side (fiber optic grade epoxy, EpoTek 377, EpoTek) to another cleaned piece of Si wafer, and the epoxy cured at 150 °C for 30 min. To minimize the effect of surface

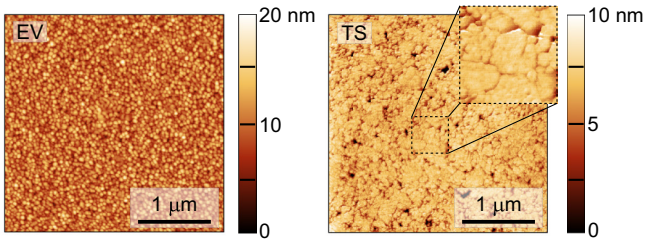


FIG. 2. (Color online) AFM topography of evaporated (EV) and template-stripped (TS) silver surface, with root mean square (rms) surface roughness of 2.4 nm and 1.2 nm, respectively. The average grain size for EV is about 50 nm and that for TS is about 100 nm as derived from the Fourier transform analysis of the topography image.

oxidation [67], samples are then stripped to expose the Ag film but only shortly before the measurement.

Template stripping is preferred over other methods for sample preparation, because of the reduced surface roughness and larger grain size [68]. In addition, the final metal surface remains protected from oxidation and contaminations from atmosphere prior to measurement.

The TS silver films are carefully characterized for surface defects. Dark-field optical microscopy is used for inspection over the whole sample surface, noting no visible defects. For local-area characterization, the samples are analyzed by noncontact atomic force microscopy (AFM, Innova, Bruker), shown in Fig. 2. Root mean square (rms) surface roughness of 1.2 nm was obtained for TS silver with estimated average grain size of 100 nm, comparable to the best literature values [23,31,68]. For comparison, the evaporated Ag side before template stripping exhibits rms roughness of 2.4 nm and grain size of 50 nm. For direct comparison and to test consistency with our earlier work [16], we also measured the dielectric function of gold. TS gold samples were prepared in the same way as the silver samples.

In contrast to standard reflectivity methods which only record the intensity, spectroscopic ellipsometry provides direct access to the complex dielectric function from two independent parameters [69]. Ellipsometry relies on the measurement of the ratio of complex reflectance $\rho$, given by the ratio of reflection coefficients for $p$ and $s$ polarization

$$\rho = r_p/r_s = (\tan\Psi)e^{i\Delta}, \tag{7}$$

with amplitude ratio $\tan\Psi$ and phase difference $\Delta = \phi_p - \phi_s$. By measuring only the relative reflectivities of different polarizations, ellipsometry does not require a reference sample or Kramers-Kronig analysis [48,69]. The nature of measuring relative values also makes the method robust to intensity fluctuations of the source.

We used two variable-angle spectroscopic ellipsometers (VASE and IR-VASE, J. A. Woollam). VASE (variable-angle spectroscopic ellipsometer) for the spectral range from 0.62 eV to 4.14 eV (2 $\mu$m–300 nm) uses a xenon lamp with a monochromator. IR-VASE, covering 0.05–0.73 eV (25–1.7 $\mu$m), uses a glow bar and is based on a Fourier-transform spectrometer.

According to the manufacturer calibration, the accuracy of both instruments tested in transmission without a sample loaded is better than $\delta\Psi = \pm 0.14^\circ$ and $\delta\Delta = \pm 0.8^\circ$ for IR-VASE, and $\delta\Psi = \pm 0.03^\circ$ and $\delta\Delta = \pm 0.2^\circ$ for VASE. Factory calibration for both of the instruments has been performed using a $Si/SiO_2$ calibration sample [70]. In addition, ellipsometers in two different laboratories have been cross-checked to eliminate the possibility of systematic errors as discussed previously [16].

Measurements are taken and averaged at three angles of incidence of 65°, 70°, and 75°. To further reduce noise, long measurement times of 5 hours for IR and 3 hours for visible/UV lead to a statistical uncertainty $<1\%$ over the full spectral range.

The relation connecting the ellipsometry measurements to the dielectric function can be derived from Fresnel's equation, with

$$\rho = \frac{r_p}{r_s} = \left(\frac{\tilde{n}\cos\theta_0 - \cos\theta_1}{\tilde{n}\cos\theta_0 + \cos\theta_1}\right) \Big/ \left(\frac{\cos\theta_0 - \tilde{n}\cos\theta_1}{\cos\theta_0 + \tilde{n}\cos\theta_1}\right), \tag{8}$$

where $\tilde{n} = \sqrt{\tilde{\epsilon}_r}$ is the complex refractive index of the sample, and $\theta_1$ is the transmission angle which is determined by the incidence angle $\theta_0$ from Snell's law [48,69]. For a uniform, isotropic, and optically opaque material with a smooth surface the relative dielectric function $\epsilon_r(\omega)$ is directly related to $\rho(\omega)$ through

$$\epsilon_r(\omega) = \sin\theta_0^2\left[1 + \tan\theta_0^2\left(\frac{1-\rho(\omega)}{1+\rho(\omega)}\right)^2\right], \tag{9}$$

where $\theta_0$ is the angle of incidence with respect to the surface normal of the sample [3,71].

It is worth noting that the term *pseudodielectric function* is commonly used in ellipsometry to describe the effective dielectric function of bulk and surface layers for a multilayer surface model. However we retain the term dielectric function for the combined response of bulk and negligible surface contribution given the tens of nanometers penetration depth of the optical field.

An in-plane isotropic optical response is assumed for silver with negligible depolarization upon reflection at the surface. The dielectric function is therefore directly determined from the measurement of $\Delta$ and $\Psi$ using Eqs. (7) and (9). The data from this direct inversion retain the uncertainty due to instrumental errors, which we use later to characterize the error in our measurement.

Due to residual instrumental errors the data are not perfectly Kramers-Kronig consistent. We therefore fit a combination of a Drude response and three Gaussian functions to the data with good agreement over the full spectral range. A similar fitting procedure was applied in our previous work on gold [16]. We provide the raw data of both silver and our previous gold measurements in the Supplemental Material [72].

## III. RESULTS

Negative real $-\epsilon_1$ and imaginary part $\epsilon_2$ of the dielectric function in the visible/UV spectral range of 1–6 eV are shown in Figs. 3 and 4, respectively. Results from three measured TS silver samples are plotted in red (A), green (B), and blue (C). The inset in Fig. 3 shows $-\epsilon_1(\omega)$ near the interband transition in a linear plot, where $-\epsilon_1(\omega)$ undergoes a sign

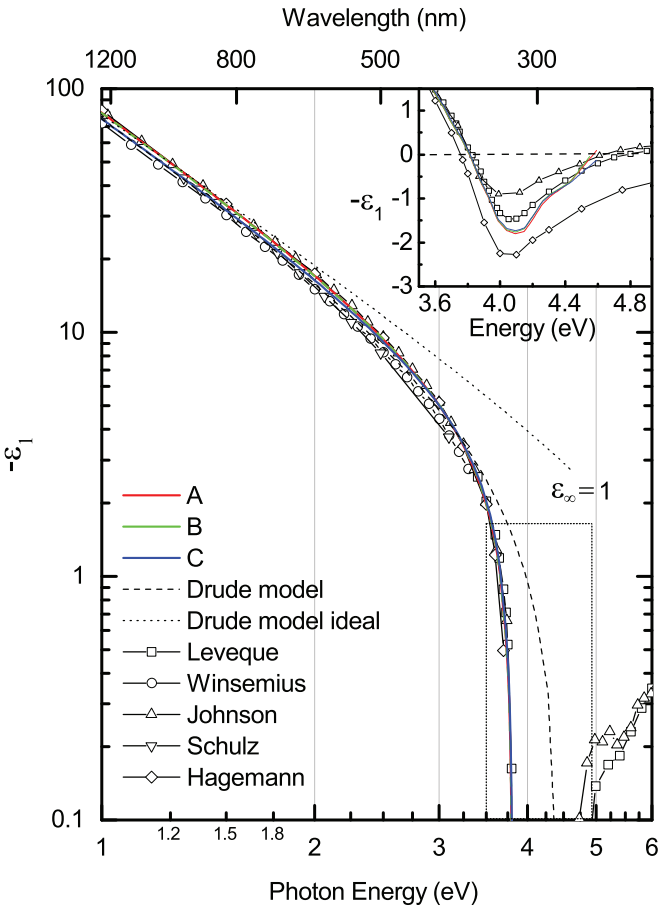


FIG. 3. (Color online) Negative real part of the dielectric function of silver $-\epsilon_1$ in the visible/ultraviolet spectral range for three different samples A (red), B (green), and C (blue). Data from Leveque *et al.* [47] (squares), Winsemius *et al.* [42] (circles), Johnson and Christy [28] (triangle), Schulz [44,45] (inverted triangle), and Hagemann *et al.* [46] (diamond) are shown for comparison. Drude fit for sample C with $\hbar\omega_p = 8.9$ eV, $\tau = 18$ fs, and $\epsilon_\infty = 5$ (dashed) or $\epsilon_\infty = 1$ (dotted line). Inset: Data near 3.8 eV shown in linear scale, where $-\epsilon_1(\omega)$ transitions from positive to negative values due to the interband transition.

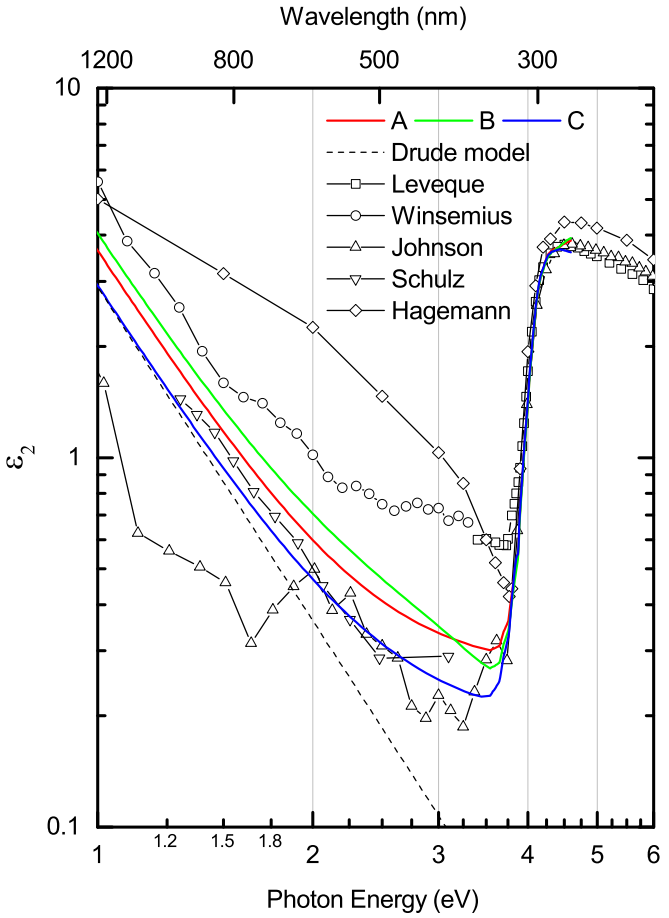


FIG. 4. (Color online) Imaginary part of dielectric function of silver $\epsilon_2$ in the visible/ultraviolet spectral range for samples A (red), B (green), and C (blue). Data from Leveque *et al.* [47], Winsemius *et al.* [42], Johnson and Christy (Johnson) [28], Schulz [44,45], and Hagemann *et al.* [46] are shown, as well as the result for the Drude model fit to sample C with parameters $\hbar\omega_p = 8.9$ eV, $\epsilon_\infty = 5$, $\tau = 18$ fs.

change due to the interband transition from the occupied $d$ band to the partially filled $sp$ band. Correspondingly, $-\epsilon_1$ and $\epsilon_2$ of the IR spectral range 0.05–1 eV are shown in Figs. 5 and 6, respectively.

In the spectral range of 1–6 eV, data for $\epsilon_1(\omega)$ and $\epsilon_2(\omega)$ from Leveque *et al.* [47] (squares), Winsemius *et al.* [42] (circles), Johnson and Christy [28] (triangle), Schulz [44,45] (inverted triangle), and Hagemann *et al.* [46] (diamond) are shown for comparison in Figs. 3 and 4. In the IR spectral range of 0.03–1 eV, Figs. 5 and 6 show data from Winsemius *et al.* [42] (circles), Johnson and Christy [28] (triangle), Dold and Mecke [41] (inverted triangle), and Bennett and Bennett [55] (diamond).

For $\epsilon_1$ the relative variations among literature values increase towards the visible spectral range, with the largest differences near the interband transition edge at ~3.8 eV. In particular, the values for $\epsilon_2$ scatter widely below 3.8 eV as seen in Fig. 4. Our data in general fall in between the results from Johnson and Christy [28], and Winsemius *et al.* [42]. Compared to [28], we have good agreement of $-\epsilon_1$, but find a considerably larger $\epsilon_2$ in the near-IR. This implies a considerably shorter value of $\tau$ compared to the results from Johnson and Christy as discussed below. Note that a careful inspection of the original data of Ref. [28] shows a large uncertainty of over 40% in $n$ in the energy range of 0.6–3 eV. As a result, with $\epsilon_2 = 2nk$, $\epsilon_2$ from Johnson and Christy scatter strongly due to the large uncertainty in $n$.

### A. Drude analysis

To obtain the Drude parameters $\omega_p$, $\epsilon_\infty$, and $\tau$, we fit our data to Eq. (4) in the range of 0.1–3 eV with a simulated annealing algorithm by minimizing the least error for $\epsilon_1(\omega)$ and $\epsilon_2(\omega)$ simultaneously [16,73]. We limit the energy range to 0.1–3 eV for the fit to minimize the effect of a frequency dependence of $\tau$ as discussed below. Above 3 eV, $\epsilon_\infty$ can no longer effectively account for the interband effects.

The fit results for samples A, B, and C are listed in Table I, with $\tau$ ranging from 15 to 18 fs for the different samples. The

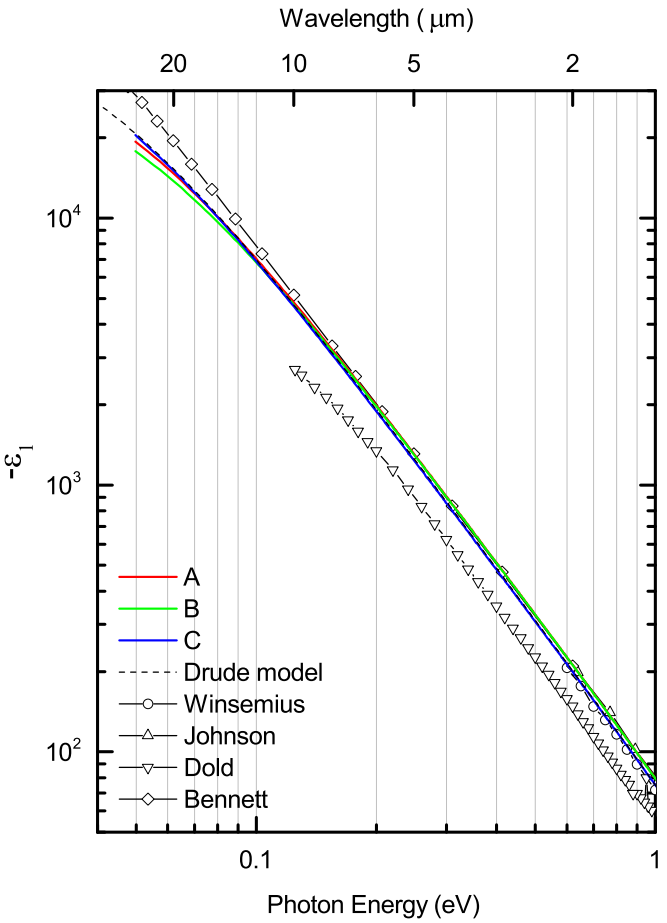


FIG. 5. (Color online) Negative real part of silver dielectric function $-\epsilon_1$ in the infrared spectral range for samples A–C (red, green, and blue). Data from [28,41,42,55] are shown together with the Drude model fit to sample C (see text).

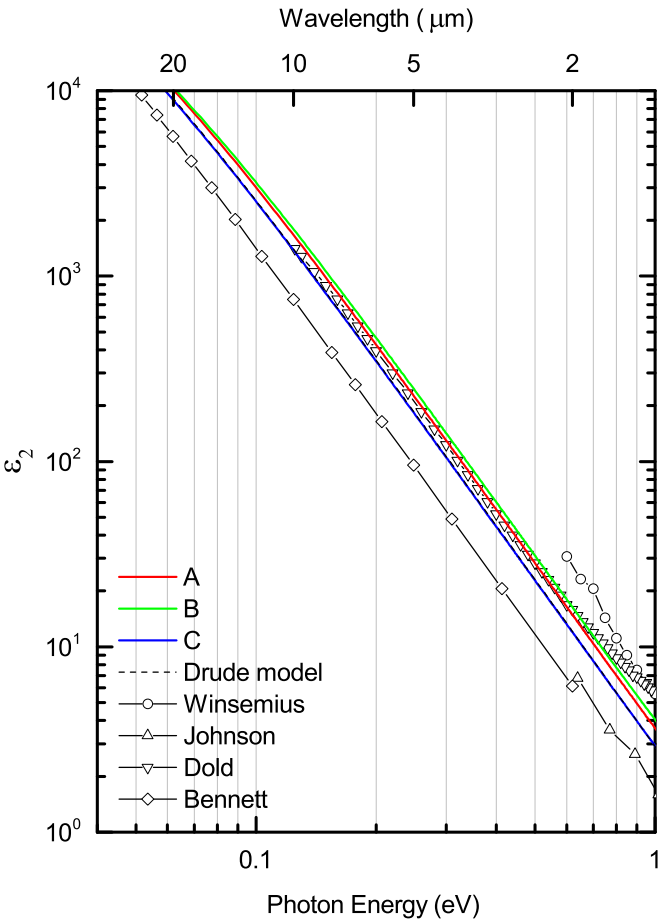


FIG. 6. (Color online) Imaginary part of silver dielectric function $\epsilon_2$ in the infrared spectral range for samples A–C (red, green, and blue) in comparison with literature from [28,41,42,55] and the Drude model fit to sample C (see text).

mean values for the three samples are $\hbar\omega_p = 8.9 \pm 0.2$ eV, $\epsilon_\infty = 5 \pm 2$, and $\tau = 17 \pm 3$ fs. The errors are calculated based on variations of the fit between the raw data and the Kramers-Kronig corrected data. The source of errors mainly come from instrumental uncertainties as discussed in Supplemental Material [72]. The dashed line in Figs. 3–6 is the dielectric function calculated for the Drude model using Eq. (4) with parameters $\hbar\omega_p = 8.9$ eV, $\epsilon_\infty = 5$, and $\tau = 18$ fs for sample C. The Drude fit has perfect agreement at low energies as expected. $\epsilon_\infty$ effectively describes the cumulative response of the bound electrons to the first order. With $\epsilon_\infty = 5$ we can describe the onset of the interband transition.

An alternative way to extract the Drude parameters is based on the approximation in Eqs. (5) and (6). In the frequency range with $\omega \gg \Gamma$ but still below the interband transition, the slope of $-\epsilon_1(\omega)$ vs $1/\omega^2$ directly provides $\omega_p^2$, the ratio of $\epsilon_2(\omega)$ vs $1/\omega^3$ gives $\omega_p^2 \times \Gamma$, and the offset of $\epsilon_1(\omega)$ extrapolated at $1/\omega^2 = 0$ provides $\epsilon_\infty$. Using this approach from 0.4–2 eV (3.1 $\mu$m–620 nm) values for $\hbar\omega_p$ of 8.7 eV, 8.9 eV, and 9.0 eV, $\epsilon_\infty$ of 6, 4, 5, and $\tau$ of 17 fs, 16 fs, and 18 fs, are obtained for samples A, B, and C, respectively. The results from the two methods are consistent.

Despite an overall good agreement with the Drude model, a deviation of the Drude fit from the direct inverted dielectric data of $\epsilon_2$ at energies below 0.1 eV and at high energies above 3 eV are noted (see Supplemental Material [72]). The deviations at high energies are due to the interband transition. The deviation of low energy $\epsilon_2$ from the Drude model is possibly due to an energy dependence of $\tau$ as predicted by Fermi liquid theory and discussed in the discussion section.

### B. Optical conductivity and skin depth

The derived complex optical conductivities $\sigma_1(\omega)$ (red) and $\sigma_2(\omega)$ (blue) from the dielectric function of sample C are shown in Fig. 7. The solid and dashed black lines are Drude fits to

TABLE I. Derived $\omega_p$,$\epsilon_\infty$,$\tau$ from Drude fit in the energy range of 0.1–3 eV for the three samples.

| | $\hbar\omega_p$ (eV) | $\tau$ (fs) | $\epsilon_\infty$ |
|---|---|---|---|
| A | $8.9 \pm 0.2$ | $17 \pm 2$ | $5 \pm 2$ |
| B | $8.9 \pm 0.2$ | $15 \pm 2$ | $4 \pm 2$ |
| C | $8.9 \pm 0.2$ | $18 \pm 1$ | $5 \pm 2$ |

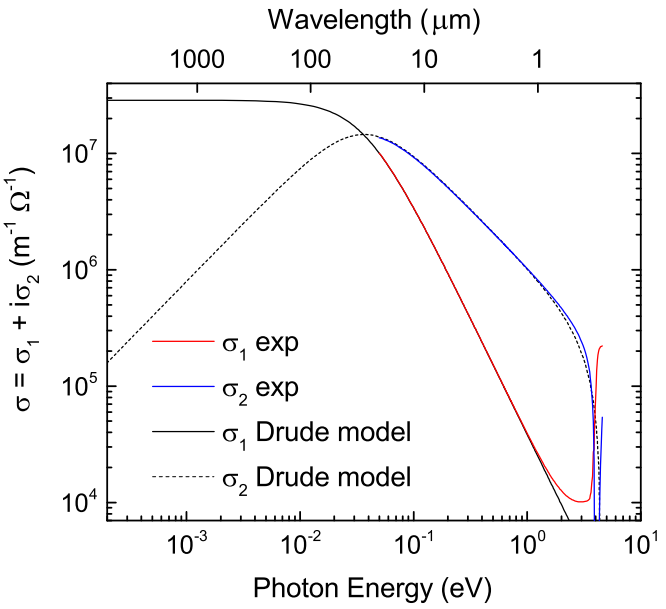


FIG. 7. (Color online) Optical conductivity $\sigma(\omega) = \sigma_1(\omega) + i\sigma_2(\omega)$ of sample C (red, blue). Drude model fit for the real part (solid black) and the imaginary (dashed black) with $\hbar\omega_p = 8.9$ eV, $\epsilon_\infty = 5$, $\tau = 18$ fs.

the real and imaginary part of the conductivity, with parameter $\hbar\omega_p = 8.9$ eV, $\epsilon_\infty = 5$, and $\tau = 18$ fs.

In the low-frequency region with $\omega\tau \ll 1$, the optical properties are mainly determined by the DC conductivity with $\sigma_{\rm DC} \approx \sigma_1 \gg \sigma_2$. Extrapolated $\sigma_{\rm DC} = 2.9 \times 10^7$ m$^{-1}$ $\Omega^{-1}$ is smaller compared to experimental DC conductivity of silver of $\sigma_{\rm DC} = 6.3 \times 10^7$ m$^{-1}$ $\Omega^{-1}$ [30]. As the frequency increases, the imaginary conductivity $\sigma_2(\omega)$ increases while the real part $\sigma_1(\omega)$ decreases and they eventually cross over near the frequency corresponding to the relaxation rate at $\omega = 1/\tau$. At even higher frequency, both $\sigma_1(\omega)$ and $\sigma_2(\omega)$ start to decrease with $\sigma_2(\omega) > \sigma_1(\omega)$ [2].

The penetration depth of an electromagnetic wave into the sample is described by the *skin depth* $\delta_0$, which is defined as the distance at which the electric field amplitude decays to $1/e$ of the incoming field amplitude. The skin depth relates to $k(\omega)$ as $\delta_0(\omega) = c/\omega k(\omega)$. Figure 8 shows the derived frequency dependence of $\delta_0(\omega)$. The skin depth remains nearly constant at $25 \pm 5$ nm in the IR, which is due to $k \propto 1/\omega$ in this spectral range. The skin depth peaks at the interband transition near 3.8 eV, where our assumption of bulklike film may fail. The peak of skin depth corresponds to a sharp minimum in $k$, which results from a particular way the dielectric function associated with the interband transitions adds to the dielectric function of the Drude free electrons (conduction electrons) in the vicinity of interband transition [6].

### C. Extended Drude model analysis

While the Drude model provides a good description of the dielectric function data across the mid-IR spectral range, a noticeable deviation between the direct inverted dielectric function $\epsilon_2$ and the Drude model prediction is seen for energies below 0.1 eV (see Supplemental Material [72]). The smaller

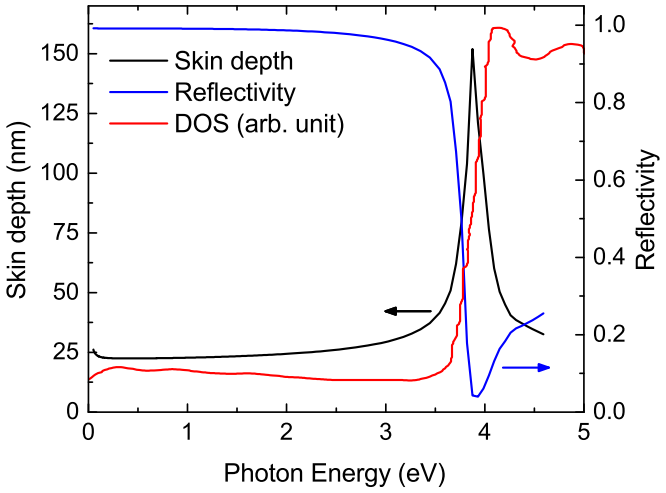


FIG. 8. (Color online) Skin depth $\delta_0(\omega)$ remains nearly constant at $25 \pm 5$ nm throughout the IR to visible range, then peaks at ~3.8 eV due to the interband transition. Derived reflectivity (blue). Density of state (DOS) from photoemission (red) [74].

experimental values for $\epsilon_2$ would suggest an increase in $\tau$ with decreasing frequency. To account for this deviation, we perform an extended Drude model analysis [36,75]. Here, the Drude parameters have frequency dependence, which can be due to electron-electron interactions [35,36,63]. After introducing a frequency dependence to the Drude parameters, the Drude dielectric function in Eq. (4) becomes

$$\epsilon_r(\omega) = \epsilon_\infty - \frac{\omega_p(\omega)^2}{\omega^2 + i\omega/\tau(\omega)^2}, \tag{10}$$

with real and imaginary parts given by

$$\epsilon_1(\omega) = \epsilon_\infty - \frac{\omega_p(\omega)^2}{\omega^2 + 1/\tau(\omega)^2}, \tag{11}$$

$$\epsilon_2(\omega) = \frac{\omega_p(\omega)^2}{\omega^2 + 1/\tau(\omega)^2} \times \frac{1}{\omega\tau(\omega)}. \tag{12}$$

Equating the common factor in the real and imaginary part, the relaxation time $\tau(\omega)$ can be expressed as

$$1/\tau(\omega) = \frac{\omega\epsilon_2(\omega)}{\epsilon_\infty - \epsilon_1(\omega)}. \tag{13}$$

The frequency dependence of $\tau^{-1}(\omega)$ can readily be calculated with an input of $\epsilon_\infty = 5$ for silver. At low frequency $\epsilon_1 \gg \epsilon_\infty$, so the exact value of $\epsilon_\infty$ does not significantly affect the resulting $\tau^{-1}(\omega)$. The frequency dependence of $\omega_p(\omega)$ can also be derived [36,76], but we do not analyze it here.

By including electron-electron interactions, a quadratic frequency dependence of $1/\tau$ is predicted by the Fermi liquid theory with $1/\tau = a + b(\hbar\omega)^2$ [35,36]. Figure 9 shows the frequency-dependent $\tau^{-1}(\omega)$ from extended Drude analysis plotted against $(\hbar\omega)^2$. The observed linear relation below the interband transition seems to support the predicted quadratic frequency dependence of $1/\tau(\omega)$. Based on a fit with $a = 0.045$ fs$^{-1}$ and $b = 0.065$ eV$^{-2}$ fs$^{-1}$ (solid line), an extrapolation to zero frequency implies a DC value of $\tau = 22$ fs for silver. Similarly, an extended Drude analysis for

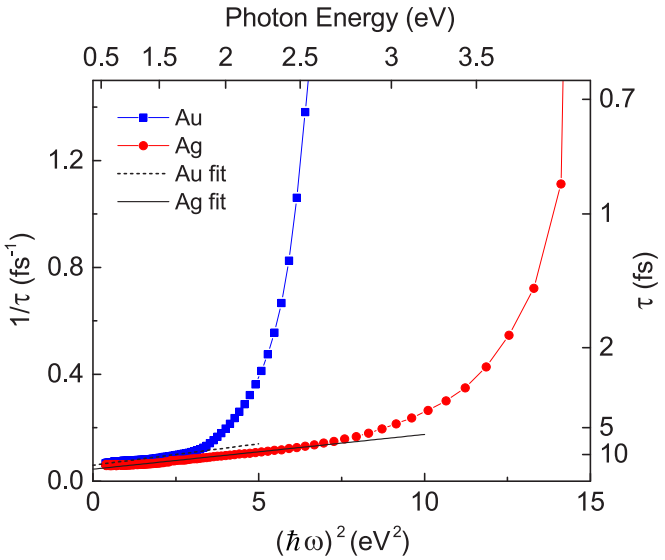


FIG. 9. (Color online) Frequency dependence of $\tau^{-1}(\omega)$ from extended Drude analysis. The linear relation below the interband transition agrees with Fermi liquid theory, $1/\tau = a + b(\hbar\omega)^2$, with $a = 0.045$ fs$^{-1}$, $b = 0.065$ eV$^{-2}$ fs$^{-1}$ for silver, and $a = 0.06$ fs$^{-1}$, $b = 0.08$ eV$^{-2}$ fs$^{-1}$ for gold, respectively. Extrapolating to zero frequency with $\tau = 22$ fs for silver and $\tau = 16$ fs for gold.

gold shows a quadratic frequency dependence of $1/\tau$ below the interband transition. A linear fit in Fig. 9 gives $a = 0.06$ fs$^{-1}$, $b = 0.08$ eV$^{-2}$ fs$^{-1}$, with extrapolated $\tau = 16$ fs at zero frequency. This value can be compared with $\tau = 13 \pm 3$ fs from the Drude analysis [16].

With closer inspection of low-frequency range of 0.05–0.1 eV, a frequency-dependent trend of $\tau^{-1}$ different than quadratic is observed. Figure 10 shows the frequency dependence of $\tau$ applying the extended Drude analysis in the

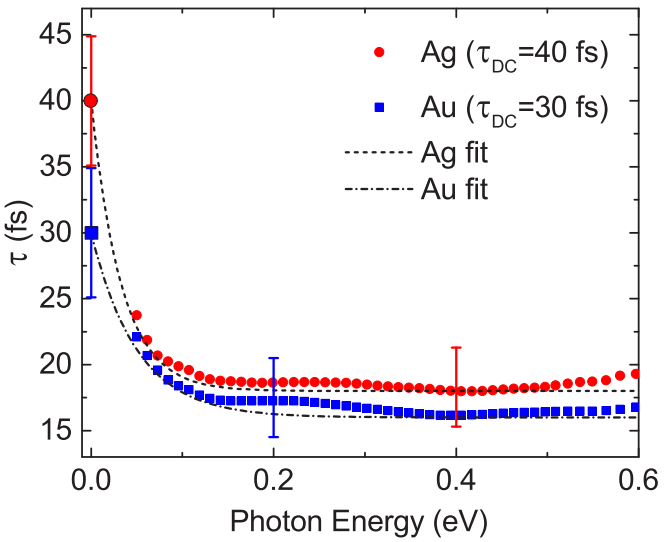


FIG. 10. (Color online) Frequency dependence of $\tau(\omega)$ in the low-energy IR range for silver (red dot) and gold (blue dot). The fits are a simple exponential connecting to the zero-frequency value of $\tau$ calculated from DC conductivity (squares) [30]. Note, however, that increase in $\tau(\omega)$ below 0.1 eV is within our instrumental error.

range of 0.05–0.6 eV. $\tau$ for silver from this work is shown in red, and $\tau$ for gold from our previous work in blue [16]. The dashed and dot-dashed line is a fit to a simple empirical exponential function with connection to the DC value (electrical relaxation time deduced from DC conductivity), for silver and gold, respectively [7,29,30]. In this plot, both $\tau$ of silver and gold indicate an exponential increase towards DC frequency, different and more rapid than the quadratic frequency dependence of $1/\tau$ from Fermi liquid theory.

## IV. DISCUSSION

### A. Comparison of Drude parameters with literature values

Our derived Drude parameters are $\hbar\omega_p = 8.9 \pm 0.2$ eV, $\epsilon_\infty = 5 \pm 2$, and $\tau = 17 \pm 3$ fs. For comparison, the range of literature values are $\hbar\omega_p = 7$–$9$ eV, $\epsilon_\infty = 1$–$10$, and $\tau = 5$–$40$ fs. The differences can be due to both instrumental errors and/or sample types and preparation procedures [16,53].

For the two previous experiments with longer $\tau$ than our measurement [28,55], some issues have already been noted above. Data from Johnson and Christy have an uncertainty of $\sim 40\%$ for $n$ in the 0.6–3 eV spectral range when $n$ is small [28]. The resulting relaxation time has a large uncertainty with $\tau = 31 \pm 12$ fs. In addition, the data directly extracted from reflection and transmission are not necessarily Kramers-Kronig consistent. Bennett and Bennett simply assumed $\tau = 36$ fs to complement their normal reflectance measurement for calculating the dielectric function in the 3–30 $\mu$m wavelength range [55]. Of the other previous measurements, data from Dold and Mecke [41] were pointed out by Lynch and Hunter [17] to have erroneously low values for $k$ resulting in too large values of $\epsilon_1$. The good agreement in $\epsilon_2$ and the difference in $\epsilon_1$ between their data and ours further imply the data from Dold and Mecke are not Kramers-Kronig consistent.

In previous experiments as well as in our measurements on three different samples, larger relative variations in visible/UV are observed in comparison to the IR region. Our derived reflectivity from the dielectric function agrees well with the behavior expected from density of state (DOS) measurements from photoemission [74], as shown in Fig. 8. The reflectivity derived from our data inversely correlates to the DOS, with good agreement on the position and slope near the interband transition.

It is in principle possible to compare the Drude parameters with results from surface plasmon resonance (SPR) lifetime measurement. $\tau$ relates to the nonradiative damping of a localized SPR, and the surface plasmon propagating length. However, SPR lifetime can be influenced by radiative damping and surface scattering, and in most nanoparticle studies, the SPR resonances spectrally overlap with interband transitions [21,22,25,77]. It is worth noting, however, that our measured $\tau = 17 \pm 3$ fs is consistent with the longest value of $\tau = 13$ fs based on plasmonic resonance linewidth of a silver nanoparticle at room temperature [21,22,25].

### B. Interband effects

As shown in Figs. 3 and 4, the experimental dielectric function deviates from the Drude behavior in the visible/UV region due to the direct interband transition from $d$ to $sp$ band.

The absorption edge in $\epsilon_2$ is very steep, and has been used to determine the starting energy of the interband transitions [78]. The different slopes of the edge from different measurements were suggested to be related to exciton-like effects or to the flatness of the $d$ band [11,29].

For energies below the onset of the interband transition, $\epsilon_\infty$ can be adjusted to partially account for the interband effect. To better describe the interband influence on the dielectric function, empirically parametrized Gaussian or Lorentzian resonances can be added into the Drude model with $\epsilon(\omega) = \epsilon_{\text{Drude}} + \epsilon_{\text{d}}(\omega)$ [59,79]. The interband contribution $\epsilon_{\text{d}}(\omega)$ can be well described by damped harmonic oscillators to parametrize the response of the $d$ electrons [79]. However, this approach does not add any additional physical insight.

### C. Deviation from Drude behavior

The Drude-Sommerfeld model (referred to as the Drude model here) recognizes the electron as a fermion and replaces the Maxwell-Boltzmann distribution in the original Drude model with Fermi-Dirac statistics. This modification changes the electron velocity distribution and related properties explicitly depending on the electron velocity, such as energy distribution and heat capacity. However, the modification does not change the expression of the dielectric function in Eq. (4) because the relaxation time $\tau$ is assumed to be independent of electron velocity in the Drude model.

Despite the general agreement between experimental results and the extended Drude model, the observed rapid rise of $\tau$ at energies below 0.1 eV cannot fully be described by the Fermi liquid theory. The relaxation time is related to the DC conductivity in the Drude model through $\sigma(0) = \epsilon_0\omega_p^2/\Gamma$. This would imply a DC conductivity of $3.6 \times 10^7$ m$^{-1}$ $\Omega^{-1}$ for $\tau = 22$ fs and $\omega_p = 9$ eV—a factor of 2 smaller than the electrically measured DC conductivity of $6.3 \times 10^7$ m$^{-1}$ $\Omega^{-1}$ [30,65,80]. Similar discrepancies between $\tau$ from optical measurements and DC resistivity measurements have been noted previously but not yet reconciled [7,29,35,62,81]. While our results suggest a connection between the IR and DC due to a rapid increase of $\tau$ below 0.1 eV, we would like to emphasize that the variation in $\tau$ below 0.1 eV is within the systematic uncertainty of our instrument when operating at the low-frequency limit.

The relaxation time $\tau$ is caused by electron damping. For an ideal silver sample free from defects and impurities at a temperature of $T = 0$ K the damping goes to zero; thus $\tau \to \infty$ [35,63]. However, for a real sample at room temperature various intrinsic and extrinsic effects result in a finite $\tau$. The relaxation rate $\tau^{-1}$, as the summed contribution from intrinsic electron-electron and electron-phonon, and extrinsic electron-surface/grain boundary scattering, can be expressed as [35,63]

$$\tau^{-1} = \tau_{\text{e-ph}}^{-1} + \tau_{\text{e-e}}^{-1} + \tau_{\text{S}}^{-1}. \tag{14}$$

$\tau_{\text{e-ph}}^{-1}$ is the dominating factor at room temperature and is a result of scattering an electron by simultaneously absorbing and emitting a phonon [35,82–84]. At frequencies much higher than the Debye frequency ($\sim 0.01$ eV), the interaction averages over all the phonon modes resulting in a constant effective collision time with negligible frequency dependence [85,86]. The contribution from electron-electron scattering has been derived as [35,87]

$$\tau_{\text{e-e}}^{-1} = \frac{\pi^3 \Sigma \Delta}{12\hbar E_F}\left[(k_B T)^2 + \left(\frac{\hbar\omega}{2\pi}\right)^2\right], \tag{15}$$

with Fermi energy $E_F$, averaged scattering probability over the Fermi sphere $\Sigma$, and the fractional umklapp scattering $\Delta$. $\tau_{\text{e-e}}^{-1}$ has a quadratic frequency dependent term. $\tau_{\text{e-e}}^{-1}$ is also quadratically temperature dependent, but the temperature dependence of electron-electron scattering is negligible compared to electron-phonon scattering at room temperature [35,87]. The interface scattering rate $\tau_{\text{S}}^{-1}$ is related to grain boundaries and surface roughness, and is assumed to be directly proportional to the surface area for nanoparticles. One therefore expects an overall quadratic frequency dependent $\tau^{-1}(\omega)$. However, the quadratic frequency dependence of $\tau^{-1}(\omega)$ can easily be obscured at finite temperature. Measurements as a function of temperature and purity, and with controlled sample morphology, are needed to discriminate the various mechanisms responsible for damping [53,63].

A reduction of relaxation rate at low temperature has been observed measuring the surface plasmon lifetimes of gold nanoparticles in agreement with theory [63]. However, the frequency dependence was not studied.

### D. Grain-size and other finite-size effects

Recently, effects of sample morphology have been studied systematically with spectroscopic ellipsometry on gold in the IR spectral range [53]. By estimating the grain size from AFM measurements, the authors established a linear relation of increasing $\tau$ with larger grain size. Their measured relaxation rate $\Gamma = 261$ cm$^{-1}$ on the sample with largest gain size of 170 nm (300 nm thick gold film on mica) corresponds to $\tau = 20$ fs. By linearly extrapolating their measurements on different samples to infinite grain size, the authors suggest $\tau = 26$ fs for gold at room temperature. This value would be close to the corresponding $\tau$ from DC conductivity of $\sim$30 fs as shown in Fig. 10, yet neglects the effects of electron-electron and electron-phonon scattering at finite temperature. At grain size of 170 nm and beyond, the relaxation time should no longer be grain size limited as the mean-free path of the electron for gold at room temperature is about 30 nm. Thus simple linear extrapolation of the relaxation time with grain size may not be valid. Variation of $\tau$ with grain size in Ref. [53] for sizes above 60 nm could also be due to differences in impurity/defect scattering due to different preparation procedures for their commercial and self-prepared samples.

We note that Ref. [53] seems to underestimate the instrumental errors. As the authors used the same type of instruments as ours, we can assign an instrumental error of 3 fs to the relaxation time $\tau$ based on our calibration which can be comparable to the differences between samples. Nevertheless their generally large values of 16–20 fs compared to our $\tau = 14 \pm 4$ fs measured for single-crystal gold and $\tau = 13 \pm 3$ fs for TS gold with average grain size of $120 \pm 30$ nm [16] would indicate higher impurity/defect scattering for our samples.

To assess sample morphology influence on silver, we compare TS silver to TS gold with similar grain size. A remeasurement on four TS gold samples on Si substrate shows good agreement with our previous TS gold measurements [16],

as well as with measurements of a 200 nm thick gold film on a polished silicon ⟨100⟩ surface in Ref. [53]. However, larger sample-to-sample variations of dielectric function $\epsilon_2$ are observed for silver. In addition, by measuring at different times of an interval of from one day up to a week after stripping, we observe that the dielectric function of TS gold varies within the uncertainty of the instruments, while similar measurements on silver show significant variations with a trend of decreasing $\tau$ over time. This suggests that the dielectric function of silver is more sensitive to variations in morphology than gold. Morphology influences on silver have also been observed with increased $\tau$ on smoother silver surface [31,37]. Measurements on a single crystal result in a larger $\tau$ than on a polycrystalline sample [26,37]. As our measurements have been performed under ambient conditions, surface oxidation is unavoidable despite great care in handling the sample. Despite numerous studies, a quantitative correlation between sample extrinsic effects and $\tau$ has not yet been performed.

### E. Conclusion

In summary, we measured dielectric function of optically thick silver film over a broad spectral range from 0.05 to 4.14 eV. Data show an overall good agreement of measured dielectric function to the Drude model. Deviation at low energies below 0.1 eV is partially explained by Fermi liquid theory with frequency-dependent Drude parameters. Sample-to-sample variations suggest the dielectric function of silver is sensitive to environmental conditions and influenced by extrinsic effects. We have improved accuracy and provided a broader spectral range compared to historical measurements, and believe our measured dielectric function is representative of high quality polycrystalline silver film in typical experimental applications. Further verification of the improvement for practical use can be tested for silver photonics applications with models based on our values. However, given the undetermined extrinsic effects more investigation is needed especially for the energy range between DC to 0.1 eV. To exclude unquantified contribution from grain boundaries, other possible surface morphology effects, and surface impurity scattering, future experiments with samples of single-crystal surfaces under ultrahigh vacuum and at variable temperature conditions are highly desirable to arrive at a more microscopic understanding of the frequency dependence of the relaxation process in metals. The possibility of different relaxation time over the Fermi surface needs to be explored by studying different surface orientations ⟨111⟩, ⟨110⟩, and ⟨100⟩. Finally, there may be a need for more direct methods, such as energy and momentum resolved photoemission, in combination with ellipsometry to probe the underlying electronic interactions of silver.

### ACKNOWLEDGMENTS

We would like to thank Dr. Robert Olmon for stimulating discussions. Funding was provided from the U.S. Department of Energy, Office of Basic Sciences, Division of Materials Sciences and Engineering, under Award No. DE-SC0008807 (sample preparation and data analysis) and from the National Science Foundation (Grant ECCS No. 1204993).

[1] N. P. Armitage, arXiv:0908.1126 [cond-mat.str-el].
[2] M. Dressel and G. Gruner, *Electrodynamics of Solids* (Cambridge University Press, Cambridge, 2002).
[3] H. Kuzmany, *Solid-State Spectroscopy* (Springer-Verlag, Berlin, Heidelberg, 2009).
[4] R. de L. Kronig, Proc. R. Soc. London A **124**, 409 (1929).
[5] R. de L. Kronig, Proc. R. Soc. London A **133**, 255 (1931).
[6] E. Taft and H. Philipp, Phys. Rev. **121**, 1100 (1961).
[7] H. Ehrenreich and H. Philipp, Phys. Rev. **128**, 1622 (1962).
[8] P. Lewis and P. Lee, Phys. Rev. **175**, 795 (1968).
[9] A. Anderson, K. S. Deryckx, X. G. Xu, G. Steinmeyer, and M. B. Raschke, Nano Lett. **10**, 2519 (2010).
[10] A. Marini and R. Del Sole, Phys. Rev. Lett. **91**, 176402 (2003).
[11] M. A. Cazalilla, J. S. Dolado, A. Rubio, and P. M. Echenique, Phys. Rev. B **61**, 8033 (2000).
[12] X. Cui, C. Wang, A. Argondizzo, S. Garrett-Roe, B. Gumhalter, and H. Petek, Nat. Phys. **10**, 505 (2014).
[13] R. D. Muiño, D. Sánchez-Portal, V. M. Silkin, E. V. Chulkov, and P. M. Echenique, Proc. Natl. Acad. Sci. USA **108**, 971 (2011).
[14] B. Gumhalter, P. Lazić, and N. Došlić, Phys. Status Solidi B **247**, 1907 (2010).
[15] J. Güdde, M. Rohleder, T. Meier, S. W. Koch, and U. Höfer, Science (New York, NY) **318**, 1287 (2007).
[16] R. L. Olmon, B. Slovick, T. W. Johnson, D. Shelton, S.-h. Oh, G. D. Boreman, and M. B. Raschke, Phys. Rev. B **86**, 235147 (2012).
[17] D. W. Lynch and W. Hunter, in *Handbook of Optical Constants of Solids*, edited by E. D. Palik (Academic Press, Burlington, 1997), pp. 275–367.
[18] M. Quinten, Z. Phys. B: Condens. Matter **101**, 211 (1996).
[19] D. J. Nash and J. R. Sambles, J. Mod. Opt. **43**, 81 (1996).
[20] C. Sönnichsen, T. Franzl, T. Wilk, G. von Plessen, and J. Feldmann, New J. Phys. **4**, 93 (2002).
[21] K. Munechika, J. Smith, Y. Chen, and D. Ginger, J. Phys. Chem. C **111**, 18906 (2007).
[22] M. Hu, C. Novo, A. Funston, H. Wang, H. Staleva, S. Zou, P. Mulvaney, Y. Xia, and G. V. Hartland, J. Mater. Chem. **18**, 1949 (2008).
[23] P. Nagpal, N. C. Lindquist, S.-H. Oh, and D. J. Norris, Science (New York, NY) **325**, 594 (2009).
[24] G. V. Hartland, Chem. Rev. **111**, 3858 (2011).
[25] M. G. Blaber, A.-I. Henry, J. M. Bingham, G. C. Schatz, and R. P. Van Duyne, J. Phys. Chem. C **116**, 393 (2012).
[26] Y. Wu, C. Zhang, N. M. Estakhri, Y. Zhao, J. Kim, M. Zhang, X.-X. Liu, G. K. Pribil, A. Alù, C.-K. Shih, and X. Li, Advanced Materials **26**, 6106 (2014).
[27] Y. Jiang, S. Pillai, and M. A. Green, Optics Express **23**, 2133 (2015).
[28] P. B. Johnson and R. W. Christy, Phys. Rev. B **6**, 4370 (1972).
[29] M.-M. Dujardin and M.-L. Thèye, J. Phys. Chem. Solids **32**, 2033 (1971).
[30] R. A. Matula, J. Phys. Chem. Ref. Data **8**, 1147 (1979).
[31] J. Hyuk Park, P. Nagpal, S.-H. Oh, and D. J. Norris, Appl. Phys. Lett. **100**, 081105 (2012).

[32] L. Zhang, A. Kubo, L. Wang, H. Petek, and T. Seideman, Phys. Rev. B **84**, 245442 (2011).
[33] A. Garcia-Lekue, J. M. Pitarke, E. V. Chulkov, A. Liebsch, and P. M. Echenique, Phys. Rev. B **68**, 045103 (2003).
[34] N. Smith, Phys. Rev. B **64**, 155106 (2001).
[35] G. R. Parkins, W. E. Lawrence, and R. W. Christy, Phys. Rev. B **23**, 6408 (1981).
[36] S. J. Youn, T. H. Rho, B. I. Min, and K. S. Kim, Phys. Status Solidi B **244**, 1354 (2007).
[37] J. H. Park, P. Ambwani, M. Manno, N. C. Lindquist, P. Nagpal, S.-H. Oh, C. Leighton, and D. J. Norris, Adv. Mater. (Deerfield Beach, Fla.) **24**, 3988 (2012).
[38] J. H. Weaver, *Optical Properties of Metals (Physik Daten)* (Fachinformationszentrum Energie, Physik, Mathematik, 1981).
[39] M. A. Ordal, L. L. Long, R. J. Bell, S. E. Bell, R. R. Bell, R. W. Alexander, and C. A. Ward, Appl. Opt. **22**, 1099 (1983).
[40] C. L. Foiles, *Metals: Electronic Transport Phenomena*, edited by K.-H. Hellwege and J. L. Olsen, Landolt-Börnstein, Group III, Condensed Matter, Vol. 15b (Springer-Verlag, Berlin, 1985).
[41] B. Dold and R. Mecke, Optik (Stuttgart) **22**, 435 (1965).
[42] P. Winsemius, F. F. van Kampen, H. P. Lengkeek, and C. G. van Went, J. Phys. F **6**, 1583 (1976).
[43] L. G. Schulz, J. Opt. Soc. Am. **41**, 1047 (1951).
[44] L. G. Schulz, J. Opt. Soc. Am. **44**, 540 (1954).
[45] L. G. Schulz and F. R. Tangherlini, J. Opt. Soc. Am. **44**, 362 (1954).
[46] H. Hagemann, W. Gudat, and C. Kunz, J. Opt. Soc. Am. **65**, 742 (1975).
[47] G. Leveque, C. Olson, and D. Lynch, Phys. Rev. B **27**, 4654 (1983).
[48] H. G. Tompkins and E. A. Irene, *Handbook of Ellipsometry*, 1st ed. (William Andrew, New York, 2005).
[49] K. Stahrenberg, T. Herrmann, K. Wilmers, N. Esser, W. Richter, and M. J. G. Lee, Phys. Rev. B **64**, 115111 (2001).
[50] D. C. Skillman, J. Opt. Soc. Am. **61**, 1264_1 (1971).
[51] H. Savaloni and M. Firouzi-Arani, Philos. Mag. **88**, 711 (2008).
[52] D. E. Aspnes, E. Kinsbron, and D. D. Bacon, Phys. Rev. B **21**, 3290 (1980).
[53] J. Trollmann and A. Pucci, J. Phys. Chem. C **118**, 15011 (2014).
[54] P. Winsemius, H. Lengkeek, and F. Van Kampen, Physica B+C **79**, 529 (1975).
[55] H. E. Bennett and J. M. Bennett, *Optical Properties and Electronic Structure of Metals and Alloys*, edited by F. Abeles (North-Holland, Amsterdam; Wiley, New York, 1966).
[56] N. W. Ashcroft and N. D. Mermin, *Solid State Physics*, 1st ed. (Brooks/Cole, Pacific Grove, CA, 1976).
[57] R. W. Boyd, *Nonlinear Optics*, 3rd ed. (Academic Press, Waltham, MA, 2010).
[58] N. E. Christensen, Phys. Status Solidi B **54**, 551 (1972).
[59] M. B. Raschke, S. Berweger, and J. M. Atkin, *Plasmonics: Theory and Applications*, edited by T. V. Shahbazyan and M. I. Stockman (Springer Netherlands, Dordrecht, 2013), pp. 237–281.
[60] A. Marini, R. Del Sole, and G. Onida, Phys. Rev. B **66**, 115101 (2002).
[61] G. Giuliani and G. Vignale, *Quantum Theory of the Electron Liquid* (Cambridge University Press, Cambridge, 2005).
[62] M.-L. Thèye, Phys. Rev. B **2**, 3060 (1970).
[63] M. Liu, M. Pelton, and P. Guyot-Sionnest, Phys. Rev. B **79**, 035418 (2009).
[64] S. Grothe, S. Johnston, S. Chi, P. Dosanjh, S. A. Burke, and Y. Pennec, Phys. Rev. Lett. **111**, 246804 (2013).
[65] D. Tanner and D. Larson, Phys. Rev. **166**, 652 (1968).
[66] W. Lawrence, Phys. Rev. B **13**, 5316 (1976).
[67] H. E. Bennett, J. Appl. Phys. **40**, 3351 (1969).
[68] E. A. Weiss, G. K. Kaufman, J. K. Kriebel, Z. Li, R. Schalek, and G. M. Whitesides, Langmuir **23**, 9686 (2007).
[69] T. W. H. Oates, H. Wormeester, and H. Arwin, Prog. Surf. Sci. **86**, 328 (2011).
[70] J. A. Woollam, VASE Ellipsometer specifications, 2007 (unpublished).
[71] J. A. Woollam, B. Johs, C. Herzinger, J. Hilfiker, R. Synowicki, and C. Bungay, SPIE Proc. **CR72**, 3 (1999).
[72] See Supplemental Material at http://link.aps.org/supplemental/10.1103/PhysRevB.91.235137 for the comparison of the Drude fit and the direct inverted raw data.
[73] S. Kirkpatrick, C. D. Gelatt, and M. P. Vecchi, Science (New York, NY) **220**, 671 (1983).
[74] G. Panaccione, G. Cautero, M. Cautero, A. Fondacaro, M. Grioni, P. Lacovig, G. Monaco, F. Offi, G. Paolicelli, M. Sacchi, N. Stojić, G. Stefani, R. Tommasini, and P. Torelli, J. Phys.: Condens. Matter **17**, 2671 (2005).
[75] R. D. Muiño, E. E. Krasovskii, W. Schattke, C. Lienau, and H. Petek, in *Dynamics at Solid State Surfaces and Interfaces*, edited by U. Bovensiepen, H. Petek, and M. Wolf (Wiley-VCH Verlag GmbH & Co. KGaA, Weinheim, Germany, 2012).
[76] J. W. Allen and J. C. Mikkelsen, Phys. Rev. B **15**, 2952 (1977).
[77] M. Bosman, E. Ye, S. F. Tan, C. A. Nijhuis, J. K. W. Yang, R. Marty, A. Mlayah, A. Arbouet, C. Girard, and M.-Y. Han, Sci. Rep. **3**, 1312 (2013).
[78] D. W. Lynch, in *Handbook of Optical Constants of Solids*, edited by E. D. Palik (Academic Press, Burlington, 1997), pp. 189–212.
[79] A. D. Rakic, A. B. Djurisic, J. M. Elazar, and M. L. Majewski, Appl. Opt. **37**, 5271 (1998).
[80] F. Pawlek and D. Rogalla, Cryogenics **6**, 14 (1966).
[81] H. Gugger, M. Jurich, J. D. Swalen, and A. J. Sievers, Phys. Rev. B **30**, 4189 (1984); **34**, 1322 (1986).
[82] T. Holstein, Ann. Phys. **29**, 410 (1964).
[83] G. Brändli and A. J. Sievers, Phys. Rev. B **5**, 3550 (1972).
[84] R. R. Joyce and P. L. Richards, Phys. Rev. Lett. **24**, 1007 (1970).
[85] H. Scher, Phys. Rev. Lett. **25**, 759 (1970).
[86] P. Allen, Phys. Rev. B **3**, 305 (1971).
[87] W. E. Lawrence and J. W. Wilkins, Phys. Rev. B **7**, 2317 (1973).